ResearchGate

See discussions, stats, and author profiles for this publication at: https://www.researchgate.net/publication/228594580

Orientation-Resolved Chemical Kinetics: Using Microfabrication to Unravel the Complicated Chemistry of KOH/Si Etching

ARTICLE *in* THE JOURNAL OF PHYSICAL CHEMISTRY B · FEBRUARY 2002

Impact Factor: 3.3 · DOI: 10.1021/jp011361j

CITATIONS
43

READS
84

4 AUTHORS, INCLUDING:

Rikard Wind
Na4B LLC
13 PUBLICATIONS **270** CITATIONS
SEE PROFILE

Helen Jones
Cornell University
2 PUBLICATIONS **52** CITATIONS
SEE PROFILE

Available from: Rikard Wind
Retrieved on: 27 January 2016

Orientation-Resolved Chemical Kinetics: Using Microfabrication to Unravel the Complicated Chemistry of KOH/Si Etching

Rikard A. Wind, Helen Jones, Michael J. Little, and Melissa A. Hines*

Department of Chemistry, Cornell University, Ithaca, New York 14853-1301

Received: April 11, 2001; In Final Form: October 4, 2001

Microfabricated test patterns are used to measure the orientation-dependent rates of KOH/silicon etching of 180 surfaces in the Si[110] zone. The concentration and temperature dependence of the reaction is quantified, and a pronounced kinetic isotope effect is observed for all orientations. Although the kinetics of the KOH etching of silicon are complicated, the magnitude of the kinetic isotope effect, the morphology of the macrosteps on vicinal Si(111) surfaces, the pronounced hydrophobicity and H-termination of the etched surfaces are all consistent with a chemical mechanism that is rate-limited by cleavage of a Si−H bond by OH^-. There is no evidence of a gross change in chemical mechanism with surface orientation. Silicon surfaces in the [110] zone can be divided into four regions of similar reactivity: vicinal Si(100), vicinal Si(110), and two types of vicinal Si(111) surfaces. Within each region, all surfaces display remarkably similar chemical kinetics. These regions are separated by morphological transitions of unknown origin. The orientations of the morphological transitions are temperature dependent, which implies that they are not associated with surface structural transitions, such as reconstructions. The etch rate of vicinal Si(111) surfaces is well fit by a simple step flow model; however, etching-induced step bunching is also observed. The observed kinetics are inconsistent with existing theoretical models of step bunching. Low miscut vicinal Si(110) surfaces have very isotropic etch rates, which are attributed to etching induced faceting. The macroscopic etch rate displays markedly non-Arrhenius behavior (the etch anisotropy actually increases with temperature!), and the concentration dependence cannot be fit by a simple empirical rate law. These phenomena are attributed to the multisite nature of the etching reaction.

I. Introduction

Aqueous bases, such as KOH, NH_4OH, and TMAH (tetramethylammonium hydroxide), are arguably the most important class of industrial silicon etchants. The popularity of these etchants is driven in large part by their extreme anisotropy (i.e. their high face-specificity). As a general rule, aqueous bases etch close-packed Si(111) surfaces orders of magnitude more slowly than other silicon surfaces. Because of this, these etchants can be used to selectively machine well-aligned Si(111) surfaces. For example, anisotropic etchants have been used to fabricate inkjet printer nozzles[1] and ultra-small vee-grooves[2] for novel microelectronic devices. Although KOH is the most widely studied etchant in this class, organic bases, such as NH_4OH and TMAH, are more commonly used in industry, because trace amounts of potassium can poison microelectronic devices.

Despite the industrial importance of anisotropic etchants, relatively little is known about the chemical origins of etchant anisotropy. This lack of knowledge is not due to a lack of interest, but rather to the inherent difficulty in studying highly anisotropic reactions. For example, the extreme anisotropy of KOH coupled with the slow etching of the (111) surfaces implies that KOH attacks Si(111) defects, such as steps and pits, much more rapidly than it attacks Si(111) terrace sites. Because of this, KOH etching of Si(111) surfaces is dominated by defect reactions (e.g., step etching)—not by etching of the majority species, the terrace site. The characterization of defect reactions is notoriously difficult. The low density of these sites coupled with their varied structure makes their spectroscopic observation and characterization challenging. Because of this, the reactivity of flat surfaces is often mistakenly attributed to the reactivity of the majority species: the terrace site.

Kinetic studies of anisotropic etchants are also complicated by a more subtle morphological problem. Most kinetic investigations start with the determination of the empirical rate law. For example, Seidel and co-workers[3] showed that the rate of Si(100) etching by KOH is proportional to $[H_2O]^4[OH^-]^{0.25}$. But how should this observation be interpreted? Does this rate law reflect the molecularity of one or more elementary reactions? This question is difficult to answer unequivocally, because the macroscopic etch morphology is itself concentration dependent. As we will show later, some KOH concentrations lead to rough surfaces, others to smooth surfaces. On an atomic scale, changes in macroscopic etch morphology imply dramatic changes in step and defect densities. These changes in defect density complicate the kinetic analysis. Is the observed rate law due to the inherent concentration dependence of the etching reactions or does it also reflect concentration-dependent changes in defect density (i.e., etch morphology)?

To ameliorate problems such as these, we take a different approach to kinetic measurements in this study: an *orientation-resolved* approach that attacks the problem of defect reactivity geometrically. Using a recently developed technique that relies on micromachined test patterns,[4] we simultaneously measure the etch rates of an array of surfaces that differ only in their surface miscut. The surface miscut controls the (initial) density

* Corresponding author. E-mail: Melissa.Hines@cornell.edu. Phone/FAX: 607-255-3040.

10.1021/jp011361j CCC: $22.00 © 2002 American Chemical Society
Published on Web 01/29/2002

of surface defect sites (i.e., steps). These arrays are subjected to the usual battery of kinetic experiments. In particular, we study the effects of temperature, etchant concentration and isotopic substitution on etch rate and correlate changes in chemical kinetics with changes in macroscopic etch morphology, as observed with electron and optical microscopies.

In the following, we show that the dramatic, orientation-dependent changes in surface morphology that are produced by KOH etching of silicon are correlated with pronounced changes in chemical kinetics.

A. The Chemistry of KOH Etching of Silicon. Although the chemical reactions underlying KOH/Si etching are controversial, it is generally accepted that KOH etching produces a hydrogen-terminated surface. The most direct evidence for this comes from the vibrational spectrum of etched, close-packed surfaces. For example, the infrared spectrum of etched Si(111) and Si(100) surfaces display a strong absorption in the Si−H stretch region and little to no absorption in the O−H stretch region.[5−7] Taken together, these features are indicative of a H-terminated surface with little to no surface oxidation. The absence of subsurface oxidation is confirmed by the lack of a strongly blue-shifted Si−H stretch, which would indicate back-bond oxidation.[8] Although vibrational studies have been restricted to the close-packed planes of silicon, the marked hydrophobicity of all KOH-etched silicon surfaces strongly suggests that all orientations are H-terminated by the etchant. [Oxidized silicon surfaces are extremely hydrophilic. The correlation between hydrophobicity (water contact angle) and surface oxidation state has been quantified using X-ray photoemission spectroscopy.[9]]

There is general agreement that KOH etching of silicon involves a number of sequential reactions. Some of these reactions are redox reactions, as two H_2 molecules are produced per etched atom.[10] The rate of etching is also dependent on KOH concentration; pure water does not dissolve silicon at an appreciable rate. Therefore, KOH etching of silicon involves *at least three reactants*: OH^-, H_2O, and silicon. One possible net etching reaction, which was suggested by Palik and co-workers,[10] is

$$Si + 2\,H_2O + 2\,OH^- \rightarrow 2\,H_2 + Si(OH)_2O_2^{-2} \qquad (1)$$

This reaction is obviously incomplete, though, as it does not explain the H-termination of the surface. A more complete discussion of previous work and possible mechanisms is presented in ref 4.

Because of its technological importance, the kinetics of KOH/Si etching—especially the KOH concentration dependence—have been studied on close-packed surfaces by many researchers. For example, Glembocki et al.[11] showed that the rate of Si(100) etching reaches a maximum at an intermediate KOH concentration (~ 6 M or 30% w/v). Since the concentration of water is substantially lowered at high KOH concentrations, this maximum is qualitatively consistent with a reaction requiring both OH^- and H_2O.

B. Orientation-Resolved Chemical Kinetics. The reactivity of a series of miscut surfaces can potentially contain much more information than the reactivity of a single surface. For example, Figure 1 shows the orientation-dependent etch rate of 90 different silicon surfaces in the Si[110] zone etched in 70 °C, 50% (w/v) KOH.[12] The miscut angle ϕ is measured with respect to one of the Si(111) faces in the zone. The etch rate shows a pronounced minimum at the close-packed Si(111) faces. In a previous publication, we showed that this minimum is consistent with simple step flow etching. To first approximation, a vicinal surface with reactive steps and completely unreactive terraces should have a macroscopic etch rate, R, that is proportional to the step density,

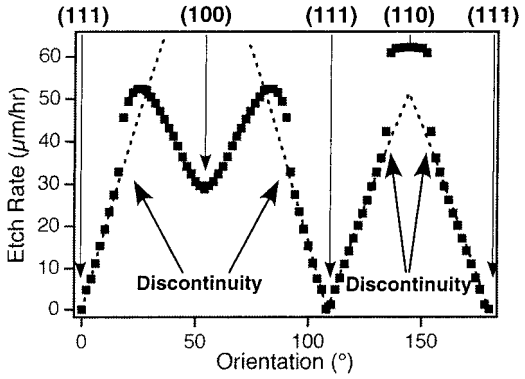

Figure 1. The orientation-dependent etch rates of 90 surfaces in the Si[110] zone. The miscut angle ϕ is measured with respect to one of the Si(111) faces in the zone. The dotted lines represent the best fit of the vicinal Si(111) etch rates to eq 3.

$$R(\theta) = v_{step} \sin|\theta| \qquad (2)$$

where θ is the miscut angle measured from the close-packed plane, and v_{step} is a constant describing the rate of step etching. The geometrical factor accounts for the change in step density with miscut angle. To qualitatively account for the finite etch rate of the close-packed plane (i.e., $\theta = 0$), a second term must be added, yielding

$$R(\theta) = v_{step} \sin|\theta| + v_{terr} \cos\theta \qquad (3)$$

where v_{terr} is a constant that qualitatively describes the rate of terrace etching.

As we will show, the KOH etch rates of vicinal Si(111) surfaces are well reproduced by this simple equation over a wide range of temperatures and concentrations. Since the atomic structure of steps on a vicinal Si(111) surface is dependent on the miscut direction, two different values of v_{step} are needed to describe the regions $\phi < 108°$ (i.e., miscut toward $\langle\bar{1}\bar{1}2\rangle$) and $\phi > 108°$ (i.e., miscut toward $\langle 11\bar{2}\rangle$). Taking this into account, the dotted line in Figure 1 represents the best fit of the experimental data to eq 3. Since this simple model is in excellent agreement with the experimental data over a large range of angles [± 20° of Si(111)], we previously concluded that step etching dominates the reactivity of vicinal Si(111) surfaces in 50% KOH. Because of this, the rate of step etching can be measured from the orientation-dependent etch rate using eq 3. Of course, this analysis does not allow us to distinguish between the different possible reactive sites on the steps. The good fit is consistent with fast etching step sites, fast etching kink sites or some combination of the two.

Vicinal Si(100) surfaces show a similar orientation-dependent behavior; however, the shallowness of the (100) minimum suggests that the etching of terrace sites plays a significant role in vicinal Si(100) etching. Since eq 3 only includes contributions from *vicinal steps*, a fit to this equation may not yield a reliable estimate of the rate of step etching. Steps that are nucleated by terrace site etching (i.e. steps that enclose etch pits) are not included, as they do not have a simple geometric dependence. This oversimplification accounts for the lack of a true cusp in the experimental data at the (100) orientation, as verified by atomistic simulations of site-specific etching.[4]

Although this simple model explains the appearance of cusps and minima at close-packed planes, it does not explain other

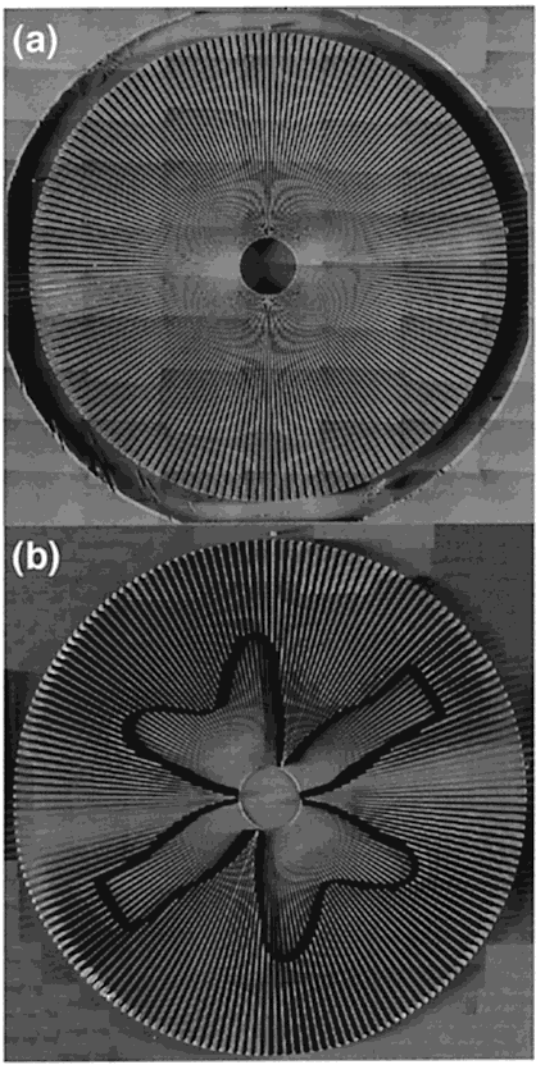

Figure 2. Composite optical micrographs of micromachined test patterns. (a) Before etching. (b) After etching in a 70 °C, 50% w/v KOH solution. The entire pattern is 18 mm in diameter.

features in the observed anisotropy. In particular, the pronounced discontinuity in the etch rate near Si(110) and the weaker discontinuity between the Si(111) and (100) orientations are very puzzling. As we will show, both of these discontinuities are accompanied by a pronounced change in macroscopic surface morphology. The isotropic etching of vicinal Si(110) surfaces is also surprising. In the following, we will show that this isotropy is likely explained by etching-induced faceting, not by isotropic atomic scale reactions.

II. Experimental Section

Silicon etch rates are highly temperature and concentration dependent. Because of this, accurate orientation-dependent kinetic measurements require a technique that is either extremely reproducible, enabling the serial measurement of many different orientations under identical conditions, or highly parallel, allowing the simultaneous measurement of many orientations under exactly the same kinetic conditions. We adopted the latter approach and used a micromachined test pattern that we recently developed.[4]

The test pattern used in this work is slightly modified from our original publication. As before, the test pattern consists of 180 1°-wide, 140 μm tall, equidistantly spaced wedges arranged in a circular array as shown in Figure 2(*a*). In this work, we increased the spacing between each wedge over that reported in ref 4 by radially offsetting each wedge by 1 mm from the center point. This geometric expansion increases the separation between adjacent wedges by an additional 34 μm. The pattern is fabricated from a single-crystal B-doped, 10 ohm cm Si(110) wafer using standard micromachining techniques. Since the pattern is fabricated from a Si(110) wafer, the sides of the wedges are composed of many surfaces in the Si[110] zone, including all of the important close-packed faces of silicon: Si(100), Si(111). and Si(110).

Before etching, the micromachined patterns are chemically cleaned using a variant of the RCA standard clean as described previously.[4] Immediately following the cleaning process, etchant anisotropy is assayed by placing the test pattern in a thermostatically controlled (±0.5 °C), unstirred sample of etchant. In the experiments reported here, the etchant was composed of various mixtures of electronics-grade KOH (50% w/v aq., LabChem), reagent grade KOD (40% w/w in D_2O, Isotec), reagent grade D_2O (99.9 atom % D, Aldrich) and ultrapure water (Millipore Milli-Q).

When the pattern is immersed in the etchant, the sides of each wedge etch with a characteristic, face-specific rate. As a result, the wedges become narrower. When the sides of a wedge are etched by a distance Δt, simple geometry requires that the length of the wedge l be reduced by a distance

$$\Delta l = \Delta t \cot(\alpha/2)$$
$$= 115\Delta t \quad \text{for } \alpha = 1° \tag{4}$$

This geometrical amplification of the etch depth, Δt, facilitates accurate measurement. For example, a typical silicon etch rate of 10 μm/hr results in a wedge retraction rate of ≈1 mm/hr: a retraction rate that is easily quantified with optical microscopy.

Anisotropic etching leads to the development of a characteristic flower pattern as shown in Figure 2b. Since the maximum silicon etch rate varies from 5 to 170 μm/hr over the range of 30−90 °C, etch times ranging from 20 min to 12 h are required for accurate measurements. After etching, the flower pattern is quantified by optical microscopy and image analysis. As shown in a previous publication,[4] the flower pattern can be directly and quantitatively inverted to obtain the orientation-dependent etch rates. Etch rates measured by this technique are in good agreement with those measured using traditional means. Thus, constrained fluid flow between the wedges does not affect our measurements.

Before etching, all surfaces on the micromachined test pattern are smooth when viewed in a scanning electron microscope (SEM); however, characteristic etch morphologies develop on the sides of some of the wedges during KOH etching. The morphology of the etched wedges was imaged with a SEM. Since the micromachined surfaces are very narrow (≤140 μm), we performed a limited number of control experiments on macroscopic miscut silicon samples (≈1 cm^2) to test for boundary induced artifacts. In every orientation tested, the etch morphology of the micromachined surface appeared to be identical to that of the macroscopic sample, and no evidence of boundary effects was ever observed.

The results presented in this paper are symmetry averaged. Because of this, we refer to all geometrically equivalent surfaces by their "principal" name. For example, wedges with $(\bar{1}11)$, $(1\bar{1}1)$, $(11\bar{1})$, and $(\bar{1}1\bar{1})$ sidewalls are formed on Si(110) surfaces; however, we refer to all of them as (111) faces. Additionally, our data are typically averaged over 2−4 replicate experiments.

III. Results and Discussion

When silicon is etched in 50% KOH at 70 °C, two striking and unexpected features appear in the orientation-dependent etch rate. First, the etch rate displays two apparent discontinuities: a pronounced discontinuity near the (110) orientation and a smaller discontinuity between the (100) and (111) orientations, as indicated in Figure 1. Second, the etch rate of vicinal Si(110) surfaces is orientation-independent up to a critical miscut. Neither one of these features can be explained in terms of simple step and terrace etching.

In the following, we investigate the origins of these unusual features using orientation-resolved chemical kinetics experiments. As our interest was initially piqued by data taken in 50% KOH, most of our experiments have been performed at this concentration; however, we have also performed a limited set of experiments at lower concentrations.

A. The Correlation between Etch Morphology and Etch Rate Discontinuities. The morphology of surfaces etched in 50% KOH is surprisingly sensitive to surface orientation, as illustrated by the sides of the etched wedges in Figure 3. The etched surfaces fall into one of two categories: either the surfaces are smooth and featureless, or they display characteristic, micron-scale surface features. The transition between rough and smooth morphologies is sudden. Figure 3 shows that very rough morphologies are often adjacent to extremely smooth morphologies, even though these surfaces differ by a mere 2° in orientation. Although the morphological transitions occur at well defined and reproducible orientations, the orientations at which the transitions occur are dependent on both the etchant temperature and the etchant concentration (vide infra).

The morphological transition is also reflected in the chemical kinetics, as the boundary between the two morphological regimes always coincides with the etch rate discontinuity. The correlation between surface morphology and etch rate is sketched in Figure 4. In 50% KOH, the fast etching orientations near the (110) and (100) planes are always smooth (as measured by SEM), while the slow etching orientations around Si(111) are rough. [The Si(111) wedge itself etches extremely slowly and remains smooth.] At lower KOH concentrations, small miscut Si(110) surfaces continue to display orientation-independent etch rates, but they also develop a characteristic facetted structure. Within the rough regions, the etch morphologies are also orientation dependent. For example, low miscut vicinal Si(111) surfaces display meandering, steplike features or "macrosteps" (e.g., Figure 5a−d) that are typically hundreds of nanometers in height (as measured by AFM). In contrast, highly miscut Si(111) surfaces near the (110) transition display characteristic pyramidal features (e.g., Figure 3b,c), while those near the (100) transition also display macrosteps (e.g., Figure 3d).

In the remainder of this section, we will discuss macrostep formation on low-miscut Si(111) surfaces and then present a morphological explanation for the isotropic etch rates of low-miscut Si(110) surfaces. In succeeding sections, we will use orientation-dependent kinetic measurements to probe the possible origins of these features.

1. Vicinal Si(111) and the Development of Macrosteps. The formation of macrosteps on etched vicinal Si(111) surfaces is very surprising given the good agreement between the orientation-dependent etch rates and the step flow etching model (i.e., eq 3). This good fit implies that the rate of step etching is *independent of step density* over a wide range. As we shall discuss, this observation apparently contradicts current theories of macrostep formation.

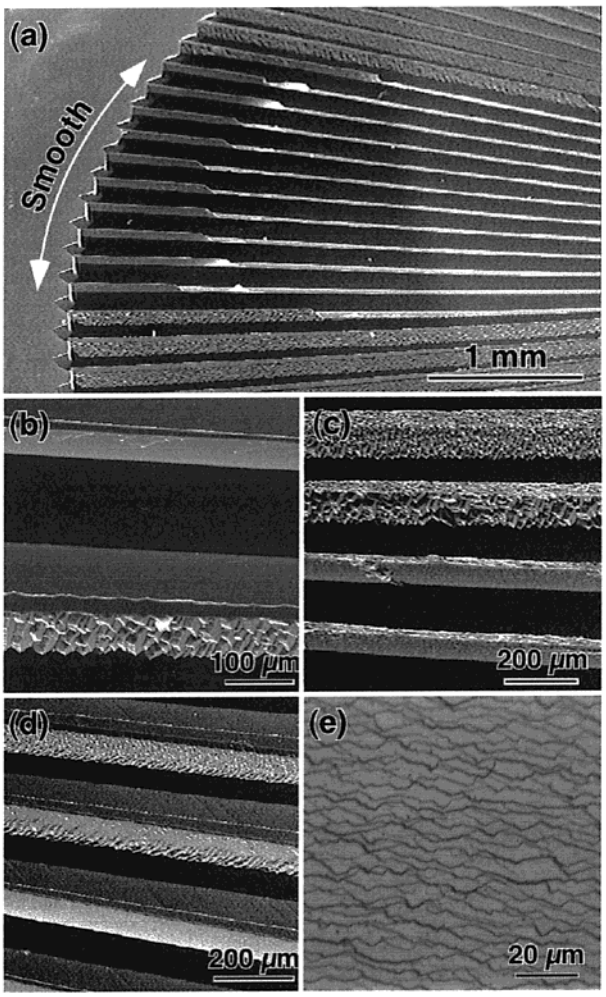

Figure 3. The etched surfaces display characteristic, orientation-dependent morphologies as shown by SEM micrographs of the sides of the etched wedges. (a) Low miscut vicinal Si(110) surfaces etched in 90 °C, 50% KOH have smooth morphologies and an orientation-independent etch rate. Past a critical miscut, the etch rate drops discontinuously, and the etched surfaces become rough. (b) A higher magnification view of the transition in (a), showing one rough and one smooth wedge. (c) Vicinal Si(110) surfaces etched in 50 °C, 50% KOH display a transition similar to that in (*a*) albeit at a different orientation. (d) Vicinal Si(100) surfaces etched in 90 °C, 50% KOH also display a morphological transition at the etch rate discontinuity. (e) Optical micrograph of Si(111) wafer miscut by 7° toward $\langle\bar{1}12\rangle$ etched in 70 °C, 50% KOH displays formation of macrosteps. Similar morphologies are seen on etched wedges of this orientation, implying that boundary effects do not cause morphological features.

The first and by far the most commonly invoked theory of macrostep (or hillock) formation is a one-dimensional model of step flow etching that was proposed essentially simultaneously by Frank,[13] who described growth hillocks, and by Cabrera and Vermilyea,[14] who described etch hillocks. Both of these theories were based on *kinematic waves*,[15] a mathematical construct developed by Lighthill and Whitham to describe river flow. These theories have been reviewed previously.[16]

In kinematic wave theory, etching is only allowed at step sites, and the etch rate of an individual step v_{step} is assumed to be only a function of the *local* step density ρ_{step}. Mathematically, $v_{step} = f(\rho_{step})$. If the steps etch independently (i.e., there are no step-step interactions and $\partial v_{step}/\partial \rho_{step} = 0$), all steps will move with the same velocity, independent of local step density and miscut. Under these kinetics, a perfectly smooth surface will

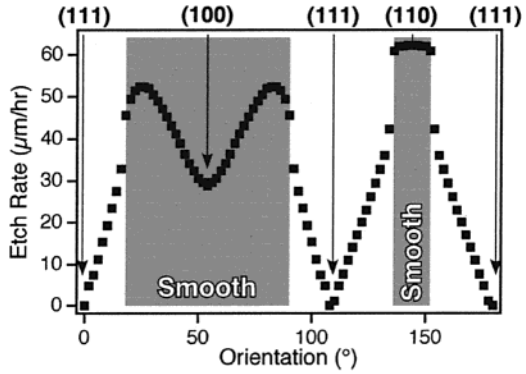

Figure 4. The transition between rough and smooth etch morphologies in 70 °C, 50% KOH occurs at the same orientation as the etch rate discontinuities.

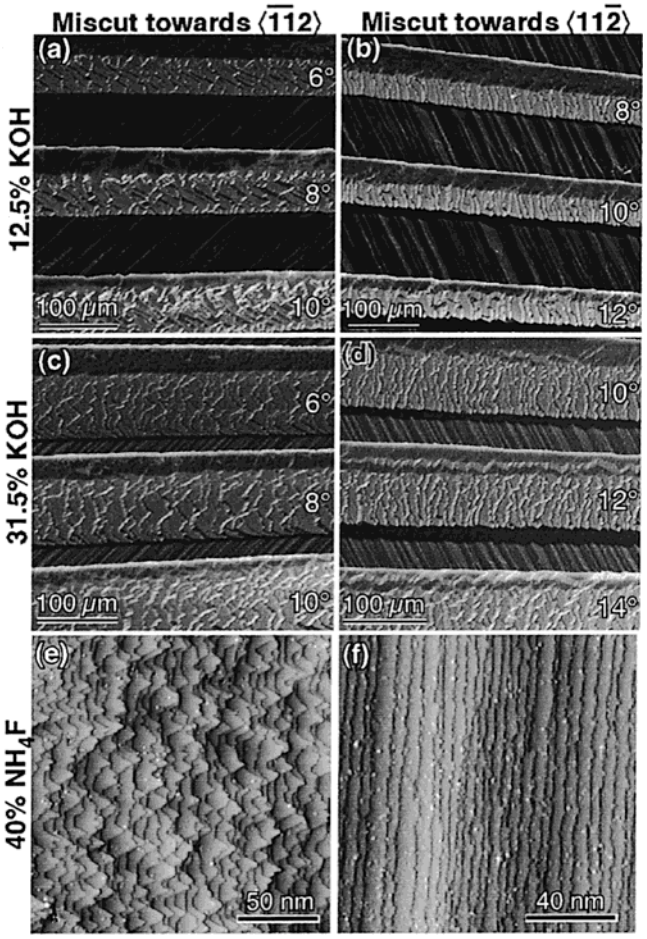

Figure 5. The etching of vicinal Si(111) surfaces in two basic solutions leads to the formation of characteristic step/macrostep morphologies. Surfaces miscut in the $\langle 11\bar{2}\rangle$ direction have steps/macrosteps with V-shaped protrusions, while those miscut in the $\langle 112\bar{}\rangle$ direction do not. (a−d) SEM micrographs of micromachined wedges etched in KOH which display ∼200 nm tall macrosteps. (e, f) STM micrographs of 3.5° miscut Si(111) wafers etched in NH_4F display atomic-height steps.

continuously roughen with etching; however, macrosteps will not form. Macrosteps will, in fact, be unstable.

Kinetic Monte Carlo (KMC) simulations of two-dimensional surfaces support this conclusion.[17] In the absences of inhomogeneities (e.g., etchant depletion and temperature gradients), atomistic simulations of simple step flow etching have shown that steps do not spontaneously bunch even when terrace etching is included. Under these conditions, individual etching steps *dynamically repel* one another over a wide range of kinetic parameters. As a result, prolonged etching in a homogeneous environment should produce a surface with roughly equally spaced atomic steps—a macroscopically smooth surface.

According to kinematic wave theory, individual steps will only bunch if the step velocity is step-density dependent. For example, consider a case of very rapid step-flow etching in which the etchant is somewhat depleted in the vicinity of each etching step. This depletion would be enhanced in regions of locally high step density. Not surprisingly, this situation leads to step bunching in much the same way that slow drivers lead to traffic jams. When a random fluctuation brings two steps close to one another (i.e., ρ_{step} locally increases), enhanced depletion in the vicinity of the step pair causes the pair to etch more slowly (i.e., v_{step} decreases). This allows the step behind the pair to catch up, which leads to slower etching of the step triad, and so on. Mathematically, this scenario occurs when $\partial v_{step}/\partial \rho_{step} < 0$. Other situations can be envisioned in which $\partial v_{step}/\partial \rho_{step} > 0$.[16] Kinematic wave theory predicts the existence of a kinetic instability that leads to macrostep formation anytime $\partial v_{step}/\partial \rho_{step} \neq 0$.

Almost all theories of step bunching or macrostep formation require some type of step-density-dependent step velocity. This dependence can be introduced by many different physical phenomena, such as elastic strain,[18−20] anisotropic diffusion[21] (e.g., Ehrlich-Schwoebel barrier[22−24] and electromigration[25−29]), contamination,[30−33] and the buildup of reaction products.[34] Although these mechanisms differ in their details, they all have the same mathematical underpinning: *a step-density-dependent etch/growth rate*. This theoretical prediction is apparently at odds with our experiments. The good fit of the macroscopic etch rate to eq 3 implies that $\partial v_{step}/\partial \rho_{step} = 0$ over a wide range of miscuts. Additionally, given the very high concentrations of the solutions used in this investigation, significant local reagent depletion seems unlikely.

One type of step bunching does not require step-density-dependent etch rates. In a number of systems, macrostep formation has been explained experimentally[35,36] and theoretically[37,38] by the existence of a thermodynamically stable facet near the original surface orientation. For example, vicinal Si(111) surfaces form large (7 × 7)-reconstructed (111)-facets separated by step bunches at temperatures near the (7 × 7)−(1 × 1) phase transition.[35] This type of facet-driven macrostep formation leads to very straight macrosteps that bound well-defined facets.

A facet-driven mechanism is inconsistent with our observed morphologies. For example, surfaces miscut toward the $\langle 112\bar{}\rangle$ direction form meandering macrosteps with many V-shaped protrusions, as shown by Figure 5a,c. Interestingly, the protrusions on these macrosteps resemble features seen on single-height atomic steps produced by NH_4F etching of similarly miscut Si(111) surfaces (Figure 5e). Surfaces miscut toward the $\langle 11\bar{2}\rangle$ direction etch to form meandering macrosteps *without* V-shaped protrusions. Again, the morphology of these macrosteps resembles the morphology of similarly miscut surfaces etched in NH_4F (Figure 5f).

Even though the driving force for the bunching is not understood, the morphological similarities between the macrosteps produced by KOH etching and the single-height steps produced by NH_4F etching suggest a similarity in chemical mechanism. Both of these etchants produce H-terminated surfaces. Previous investigations of NH_4F/Si(111) etch morphologies[39] have shown that the morphology of the etched steps is a directly related to the site-specific reactivity of the etchant. As a result, the steady state, atomic scale etch morphology can

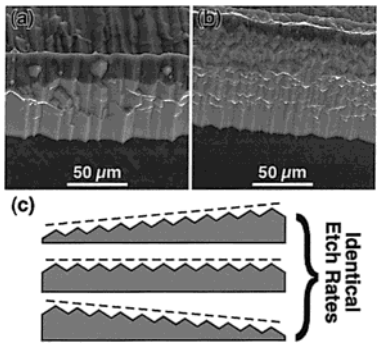

Figure 6. The etch morphology of low miscut vicinal Si(110) surfaces explains their orientation-independent etch rates. (a, b) Characteristic etching-induced faceting generates rooftop structures (a) 2° miscut Si(110) surface etched in 70 °C, 19.8% KOH. (*b*) Si(110) surface etched in 70 °C, 31.5% KOH. (c) Sketches of faceted surfaces with three different surface miscuts.

be used to extract the site-specific etch rates with the aid of kinetic Monte Carlo simulations. For example, the V-shaped etch hillocks observed on NH_4F-etched surfaces miscut toward the $\langle\bar{1}12\rangle$ direction are due to the presence of a relatively unreactive silicon dihydride species at the tip of the V which perturbs the etch kinetics.[40] On the basis of the measured site-specific reactivities, the H-termination and the known structure of the etched surfaces, NH_4F is believed to etch Si(111) via the sequential reactions:[39]

$$\equiv Si-H + OH^- + H_2O \rightarrow \equiv Si-OH + H_2 + OH^- \quad (5)$$

$$(\equiv Si)_3Si-OH + 3HF \rightarrow 3(\equiv Si-H) + SiF_3OH. \quad (6)$$

The similarity in the step morphologies suggests that the rate-limiting reaction in the KOH etching of vicinal Si(111) may be displacement of hydrogen by OH^-.

In summary, the production of macrosteps on vicinal Si(111) surfaces appears to be inconsistent with previously postulated mechanisms of step bunching and macrostep formation. The macroscopic etch kinetics imply a step-density-independent step etch rate which should not form hillocks. The absence of well-defined facets in the etch morphology is inconsistent with a facet-driven mechanism.

2. Role of Surface Morphology in Isotropic Si(110) Etching. Vicinal Si(110) surfaces etch with an orientation-independent etch rate, as shown by Figure 4. This behavior is independent of concentration (vide infra). Intuitively, this pronounced macroscopic isotropy would seem to suggest that the etchant is also isotropic on an atomic scale. In other words, this behavior suggests that all sites etch with (approximately) the same rate. At least on an atomic scale, a highly isotropic etchant would produce a rough etched surface. A close examination of the morphologies of vicinal Si(110) surfaces suggests that this is not the case. Although Si(110) surfaces etched in 50% KOH are smooth under SEM analysis, Si(110) surfaces etched in more dilute solutions develop a characteristic facetted or roof-top structure as shown by the SEM images in Figure 6. This structure is also visible on the Si(110) wafer surface visible between the wedges in Figure 4a−d.

Although we cannot explain the formation of this ridged structure, the orientation-independent etch rate can be explained by this morphology and the symmetry of the silicon lattice. As clearly seen in the symmetry of the etch pattern in Figure 2, the Si(110) surfaces possesses a mirror plane of symmetry that runs along the ridges in Figure 6a,b. Assuming that the etching-induced facets have the same orientation with respect to the lattice regardless of initial surface miscut, Figure 6c shows a cross-sectional view of three different etched surfaces. By symmetry, the atomic structures of the left- and right-facing facets sketched in Figure 6c must be identical. As a result, these three surfaces *must have identical etch rates*, even though they have different miscuts. In other words, simple geometry explains the macroscopic etch isotropy of facetted surfaces. Presumably, the surfaces etched in 50% KOH have a similar ridged structure that is too small to be observed by SEM.

This simple argument suggests that the facets formed in the etching of vicinal Si(110) surfaces all have the same orientation with respect to the silicon lattice, independent of the surface miscut. Because of the difficulty of imaging closely spaced vertical surfaces with a scanning probe microscope, we have not yet verified this prediction. Additionally, we do not know whether the facet orientation changes with etchant concentration.

3. Origin of the Morphological Transition. The formation of the ridged structure does not explain the sudden, apparently discontinuous transition between the rough and smooth etch morphologies in 50% KOH. Morphological transitions are also visible in more dilute solutions, even when the vicinal Si(110) surfaces are not smooth. To date, we have not performed a complete SEM investigation of the etch morphology at the lower concentrations.

Can these morphological transitions be explained by atomistic chemistry or are they due to mesoscale phenomena? Two very different atomistic mechanisms could explain apparently discontinuous kinetic behavior. First, a change in reactivity could be driven by a change in the rate-limiting chemical reaction. For example, if the overall etching reaction consists of sequential oxidation and etching reactions, as is often postulated in silicon etching, changes in the relative number of step and terrace sites could drive the overall reaction from oxidation-limited to etching-limited. (A transition of this type is well-known in the voltage dependence of anodic silicon etching.[41]) Second, discontinuous changes in chemical reactivity often accompany changes in surface structure. For example, if the surface spontaneously reconstructs at a particular orientation, as has been observed on clean silicon surfaces, the etch rate might show a discontinuous change. In the following sections, we will use orientation-dependent kinetic measurements to investigate (and ultimately discredit) both of these possibilities.

B. Kinetic Isotope Effect. Can the observed discontinuous change in silicon etch rate be explained by an orientation-dependent change in chemical mechanism? To address this question and probe the rate-limiting reaction, we compared the orientation-dependent etch rates of equimolar KOH/H_2O and KOD/D_2O solutions at 70 °C. Although isotopic substitution induced very little change in the *anisotropy* of the etch rate, there was a large change in absolute etch rate. On average, a 50% KOH/H_2O solution etched silicon 1.87 times faster than the corresponding KOD/D_2O solution. This is roughly consistent with the factor of 2.04 enhancement seen by Baum and Schiffrin in the etching of Si(100) at 60 °C in 2 M solutions.[42]

The orientation-dependent kinetic isotope effect was quantified using two different methods. On vicinal Si(111) surfaces where the etch rate is well fit by the simple step flow model, we extracted the rates of $\langle 11\bar{2}\rangle$ and $\langle\bar{1}12\rangle$ step etching from the best fit to eq 3 and calculated the isotopic enhancement from these rates. (On these surfaces, the rate of terrace etching is too small to be reliably estimated from our data.) As discussed earlier, this fitting procedure is not appropriate for vicinal Si(100) and Si(110) surfaces, so we performed a direct point-by-

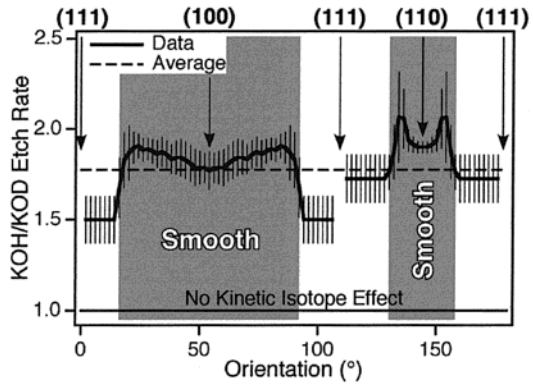

Figure 7. The orientation-dependent ratio of 8.91 M KOH/KOD etch rates showing a pronounced kinetic isotope effect. The shaded areas represent the regions of smooth etch morphology, and the transition from rough to smooth morphology is seen to coincide with a change in the isotopic enhancement. The vertical lines are 95% confidence limits.

point analysis on these orientations. Figure 7 shows our results; the vertical bars represent 95% confidence limits. A point-by-point analysis was also performed on the vicinal Si(111) data. The results of this analysis were similar, but the error bars were significantly larger due to the inherent difficulty in measuring the ratio of two small numbers.

The marked deceleration of the reaction upon deuterium substitution is consistent with a primary kinetic isotope effect.[43] This effect is quantum mechanical in nature and is primarily due to the difference in zero-point energies between X−H and X−D bonds. For example, consider the dissociation of a diatomic X−H molecule. Within the harmonic approximation, the zero-point energy of the X−H bond is $1/2\hbar\omega_{X-H}$, while the zero-point energy of the X−D bond is $1/2\hbar\omega_{X-D}$, where ω is the vibrational frequency of the molecule. Although the intermolecular potentials of the X−H and X−D molecules are identical (to first approximation), the vibrational frequencies of the isotopomers scale with their reduced mass μ according to

$$\omega = \sqrt{k/\mu}, \tag{7}$$

where k is the (isotope-independent) spring constant of the bond. This mass-dependent zero-point energy leads to a mass-dependent apparent activation barrier. If the equilibrium activation barrier (which is measured from the potential minimum) is E_{eq}, the apparent activation barrier for the (ground state) hydrogen isotopomer would be $E_{eq} - 1/2\hbar\omega_{X-H}$, while the apparent activation barrier for the deuterium isotopomer would be $E_{eq} - 1/2\hbar\omega_{X-D}$. Assuming Arrhenius behavior with an isotope-independent preexponential factor A, the relative rates of X−H and X−D dissociation, r_{X-H} and r_{X-D}, would be

$$\frac{r_{X-H}}{r_{X-D}} = \frac{Ae^{-(E_{eq}-0.5\hbar\omega_{X-H})/k_BT}}{Ae^{-(E_{eq}-0.5\hbar\omega_{X-D})/k_BT}} = e^{0.5\hbar(\omega_{X-H}-\omega_{X-D})/k_BT} \tag{8}$$

where k_B is Boltzmann's constant and T is the temperature. Since the deuterium isotopomer always has a higher effective activation barrier, this simple model predicts that the deuterium isotopomer will always be less reactive than the hydrogen isotopomer.

To the extent that cleavage of an Si−H bond can be modeled as the dissociation of a diatomic molecule of the same vibrational frequency, eq 8 can be used to predict the kinetic isotope effect resulting from an Si−H bond cleavage. The fundamental stretch vibrations of H−Si(111) and D-Si(111) have been observed at 2084 cm^{-1} and 1516 cm^{-1}, respectively.[44] Using these frequencies, eq 8 predicts a kinetic isotope effect of 3.3 for the cleavage of a silicon−hydrogen bond at 70 °C.

Although the mechanism of KOH etching of silicon is controversial, there is widespread agreement that etching follows a multistep pathway. The presence of a pronounced kinetic isotope effect in a multistep reaction implies that X−H bond cleavage occurs either before or during the rate-limiting reaction. Because of the gross oversimplifications in the derivation of eq 8, the identity of the second atom, X, cannot be determined from the magnitude of the kinetic isotope effect. In this system, the observed kinetic isotope effect could, in principle, be due to either an O−H or Si−H bond cleavage.

Since OH^- definitely plays a role in KOH etching, could diffusion of OH^- to the surface account for the observed isotope effect? At 25 °C, OH^- diffusion is faster that OD^- diffusion by a factor of 1.66.[45] Although this is roughly consistent with the measured isotopic enhancement, the highly orientation-dependent etch rates are *inconsistent* with this postulate. If OH^- diffusion were rate limiting for all orientations, the reaction rate would have to be orientation-independent as well, which it is not. The rate of OH^- diffusion could still affect the overall rate of reaction, though, if the rate of diffusion were slow enough to allow significant OH^- depletion at the surface. To account for the observed effect, etchant depletion would have to be significant at all orientations. Given the broad range of observed etch rates, this seems unlikely, so we rule out OH^- diffusion as the source of the kinetic isotope effect. Similar arguments can be made to rule out the diffusion of H_2O as the culprit.

The observed isotope effect is most likely due to a Si−H bond cleavage. As mentioned earlier, KOH-etched surfaces are predominantly, if not exclusively, H-terminated. Because of this, the initial step in KOH etching has been postulated to be

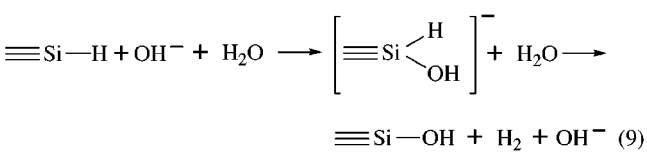

(9)

where the quantity in brackets represents the presumed pentavalent transition state. This reaction would be expected to show a primary kinetic isotope effect. In organosilicon chemistry, similar nucleophilic displacements of hydrogen by OH^- have been observed, and these reactions are believed to proceed through bimolecular, front-sided attack.[46,47] In addition, many pentacoordinate silicon anions have been observed and characterized.[48,49] Taken together, the H-termination of the surface, the pronounced kinetic isotope effect, and the morphology of the vicinal Si(111) macrosteps are all consistent with a multistep mechanism in which reaction 9 is the rate-limiting step.

The orientation dependence of the kinetic isotope effect provides additional information about the mechanism. Although the absolute etch rate changes dramatically with orientation, the kinetic isotope effect undergoes more subtle changes. The disparity in the two illustrates the utility of isotope studies. Especially in the case of surface etching, the kinetic isotope effect is a more direct diagnostic than the absolute reaction rate because isotope effects are relatively insensitive to purely morphological changes (e.g., increases in surface area). Since changes in surface morphology have a direct effect on both the surface area and the chemical composition of the surface, morphological changes directly affect the etch rate. In contrast,

the kinetic isotope effect is expected to be insensitive to morphology, because this effect is determined by the ratioed etch rates of two surfaces with similar or identical morphologies.

Taking the error bars into account, the orientation-dependent kinetic isotope enhancement suggests that silicon reactivity is divided into three, or possibly four, regions of roughly constant enhancement: the Si(100) region, the Si(110) region, and one or two regions of Si(111) step flow etching. As we shall show, other kinetic data, particularly the concentration studies, also suggest that there are four regions of chemical reactivity.

The modest changes in isotopic enhancement between these regions coupled with the pronounced hydrophobicity of the etched surfaces argue against a dramatic, orientation-dependent change in rate-limiting step. Rather, these subtle, orientation-dependent changes are more likely due to changes in the dominant reactive site participating in reaction 9. For example, a transition from step flow etching to pit nucleation and growth might correspond to a change in dominant reactive site, perhaps from kink to terrace site. The subtle difference in the isotope effect with vicinal Si(111) miscut can also be (tentatively) explained by this hypothesis, as the structure of the vicinal steps is dependent on the miscut direction. Vicinal Si(111) surfaces with $\phi < 108°$ (i.e. surfaces miscut toward $\langle\bar{1}\bar{1}2\rangle$) are expected to have dihydride-terminated steps, whereas those with $\phi > 108°$ (i.e. surfaces miscut toward $\langle 11\bar{2}\rangle$) are expected to have monohydride-terminated steps.[50]

In summary, measurements of the kinetic isotope effect are strongly inconsistent with a dramatic orientation-dependent change in chemical mechanism. Instead, these measurements suggest that the reactivity of all surfaces in the Si[110] zone are rate-limited by a reaction that involves cleavage of a Si−H bond. The subtle changes in the isotope effect with orientation are likely due to changes in the densities of the various H-terminated species on the etching surfaces.

C. Temperature Dependence and Non-Arrhenius Behavior. Since the isotopic studies are inconsistent with an orientation-dependent change in chemical mechanism, can the discontinuities in the etch anisotropies be explained by orientation-dependent changes in surface structure? There are many examples in the literature of orientation-dependent structural transitions, such as the widely studied step doubling transition on vicinal Si(100)[51] and the $(7 \times 7) - (1 \times 1)$ reconstruction transition on vicinal Si(111).[52] There are also examples of dramatic structure-induced changes in surface chemistry, such as the widely studied reconstruction-induced changes in the catalytic oxidation of CO on Pt(100).[53]

A definitive answer to this structural question would require extensive, atomic-scale studies of the etched surfaces, which is beyond the scope of this work. In the absence of such data, we will show that orientation-resolved studies of the temperature-dependent kinetics suggest that the reaction discontinuities are probably not due to orientation-dependent structural changes, such as reconstructions. We will also show that the macroscopic etch rate displays non-Arrhenius behavior, which is further evidence of the complicated, multisite nature of this reaction.

1. Temperature Dependence of the Discontinuity. If the discontinuous change in the etch morphology and etch kinetics were due to a orientation-dependent structural change (e.g., step doubling, step coalescence), we would expect that the orientation of the transition would be (at least roughly) temperature independent. To test this prediction, we measured the etch anisotropy in 50% KOH over the range of 30−90 °C. Polar plots of the temperature-dependent etch rates of silicon in 50% KOH are displayed in Figure 8a−d.

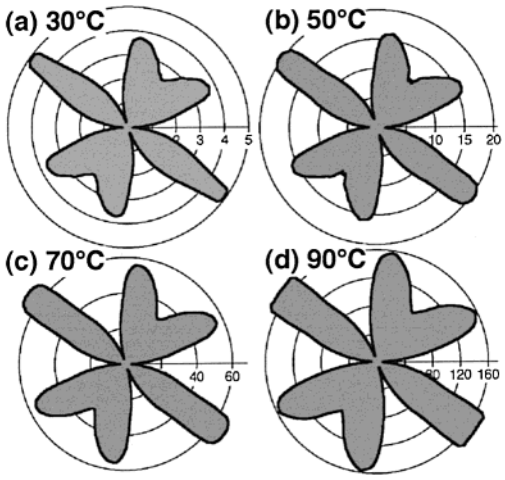

Figure 8. Temperature-dependent etch rates of silicon in 50% KOH. The etch rates are in μm/hr, and the horizontal axis denotes the Si(111) face at $\phi = 0°$.

At room temperature, vicinal Si(110) surfaces etch much faster than all other orientations, leading to two pronounced square "handles" in the anisotropy diagram. As the temperature is increased, the square handles become wider, as the position of the Si(110) discontinuity moves to higher miscut. SEM investigations of the etch morphology show that the morphological transition tracks the temperature-dependent motion of the etch rate discontinuity.

Since the orientation of the transition changes over the range 30−90 °C, the postulated structural transition would have to have an exceptionally low activation barrier to display this behavior. On clean silicon surfaces, structural transitions have much higher activation barriers. For example, the Si(111) $(7 \times 7) - (1 \times 1)$ reconstruction begins at approximately 820 °C on flat surfaces.[54] Although hydrogen adsorption may lower the barrier, the desorption of hydrogen has an activation barrier of 1.8 eV[55] and does not occur at an appreciable rate below 450 °C.[56]

Because of the silicon lattice's strongly directional covalent bonding, structural transitions at room temperature are both unprecedented and unexpected. In addition to having an unusually low activation barrier, the postulated structural transition would have to have a very unusual dependence on step density to account for the observed temperature dependence. Based on these considerations, we find it unlikely that a structural transition can account for the discontinuous change in etch rate and surface morphology.

2. Arrhenius Analysis of the Temperature-Dependent Anisotropies. Figure 9 shows the best fit activation barriers extracted from an Arrhenius analysis of the temperature-dependent anisotropies in 50% KOH. Because of the limited number of temperatures studied, an orientation-independent preexponential was assumed in the fitting procedure. As qualitatively expected from the anisotropies, the highest activation barrier corresponds to Si(111) and the lowest to Si(110). Although the error bars, which represent 95% confidence limits, are quite small, back-simulation of the data from these barriers leads to marked discrepancies between the calculated and experimental rates. These discrepancies can either be explained by pronounced, orientation-dependent variations in the preexponential factor or by non-Arrhenius behavior. In the next section, we will show that the latter is correct.

The apparent cusp in the macroscopic activation barrier at Si(111) can be qualitatively explained by simple geometry. As

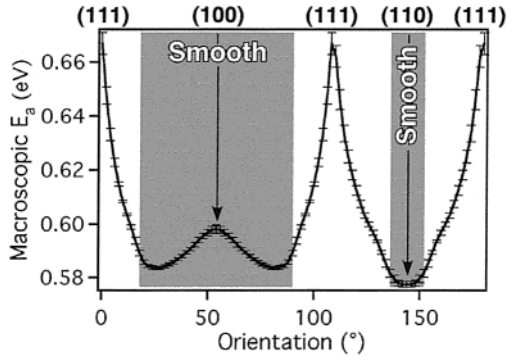

Figure 9. The apparent, orientation-dependent macroscopic activation barrier to silicon etching in 50% KOH obtained from the data in Figure 8. The shaded regions represent areas of smooth etch morphology.

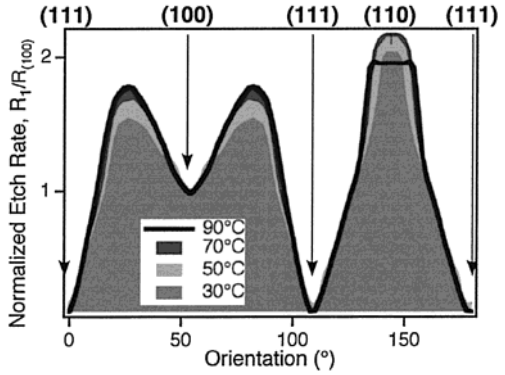

Figure 10. The normalized rate of silicon etching in 50% KOH shows that the etch rate anisotropy *increases* with increasing temperature, which is not predicted by the Arrhenius equation.

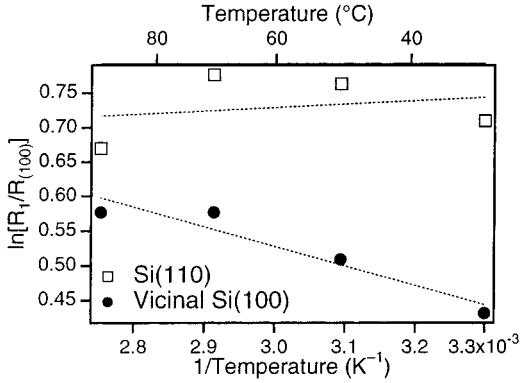

Figure 11. An Arrhenius plot of the normalized rate of Si(110) ($\phi = 144°$) and vicinal Si(100) ($\phi = 82°$) etching in 50% KOH shows that the macroscopic etch rate is markedly non-Arrhenius. The dotted lines are the best fit to the Arrhenius equation.

discussed earlier, the pronounced Si(111) etch rate minimum implies that the etching of vicinal Si(111) surfaces is dominated by step flow etching. In other words, the rate of step (or kink) site etching must be much faster than the rate of terrace etching, so $E_{step} \ll E_{terrace}$ (or $E_{kink} \ll E_{terrace}$.) Using the same geometric arguments that were used to derive eq 3, the macroscopic, miscut-angle-dependent activation barrier E_a for a vicinal Si(111) surface with a miscut angle of θ from the (111) is qualitatively given by

$$E_a = -\frac{1}{R}\frac{\partial}{\partial(1/k_BT)}R$$

$$= \frac{E_{step}e^{-E_{step}/k_BT}\sin|\theta| + E_{terrace}e^{-E_{terrace}/k_BT}\cos\theta}{e^{-E_{step}/k_BT}\sin|\theta| + e^{-E_{terrace}/K_BT}\cos\theta}$$

$$\approx \frac{E_{step}e^{\Delta E/k_BT}\sin|\theta| + E_{terrace}\cos\theta}{e^{\Delta E/k_BT}\sin|\theta|}$$

$$\approx E_{step} + E_{terrace}e^{-\Delta E/k_BT}|\theta|^{-1} \qquad \text{when } \theta \ll 1 \qquad (10)$$

where E_{step} is the activation barrier of the dominant step etching site and $\Delta E = E_{terrace} - E_{step}$. (For simplicity, a site-independent preexponential is assumed in eq 10.) This equation predicts a cusp in the macroscopic activation barrier as $\theta \rightarrow 0$ (i.e., $\phi \rightarrow 108°$.) Although the observed cusp is qualitatively described by eq 10, our simulations show that this resemblance is not quantitative.

3. Non-Arrhenius Behavior. The temperature-dependent anisotropies display strikingly non-Arrhenius behavior. Even though all of the orientation-dependent etch rates increase dramatically with temperature, as predicted by the Arrhenius equation, the *etch rate anisotropy also increases*, which is unexpected. In this system, non-Arrhenius behavior is most easily identified using etch rate ratios. The Arrhenius equation predicts that the relative etch rate of any surface normalized to the (100) surface will be given by

$$\frac{R_1(\phi)}{R_{(100)}} = \frac{A_1(\phi)}{A_{(100)}}e^{\Delta E_a(\phi)/k_BT} \qquad (11)$$

where $\Delta E_a = E_{(100)} - E_1$ is the difference in activation energies between the two surfaces, and ϕ is the miscut angle. In principle, both E_a and A are orientation dependent. If the preexponential factors are roughly equal, eq 11 predicts a uniformly decreasing anisotropy with increasing temperature. Thus, the ratioed etch rates of any two orientations should monotonically approach unity with increasing temperature, and the polar etch rate plot should become circular as $T \rightarrow \infty$. Compared to the close-packed Si(100) orientation, though, these surfaces have *increasing anisotropy* with temperature. This is most easily seen in Figure 10, where the etch rates normalized to that of the Si(100) surface are displayed. Even if the preexponential factors are different, the ratioed etch rates should follow a pseudo-Arrhenius behavior, as shown by eq 11. In contrast, Figure 11 shows that the ratioed data are strikingly non-Arrhenius.

The deviations from Arrhenius behavior are unusual and unexpected. In particular, previous studies of KOH/silicon etching have all displayed the expected Arrhenius behavior.[3,57,58] Our experiments are the first to consider the orientation-dependent etch rates specifically, and our data clearly show that the macroscopic kinetics are *non-Arrhenius.*

What is the physical meaning of these macroscopic activation barriers, if any? Previous researchers have assumed that the macroscopic barrier is related to the microscopic activation barrier of the majority species. Is the macroscopic activation barrier of the Si(111) surfaces related to the activation barrier of a terrace site to reaction 9? As we will show explicitly in an upcoming paper,[59] the correlation between macroscopic and microscopic barriers is generally quite poor. The problem is simple. Even on a nominally flat surface, etching occurs at a wide range of different sites, with each site having a different activation barrier. The macroscopic etch rate is a weighted average of the microscopic etch rates. For example, if the etching surface is composed of N different types of reaction sites (e.g., kink sites, terrace sites), and each type of site i has a surface density ρ_i, activation barrier E_i, and preexponential factor A_i,

the macroscopic etch rate R will be related to the site-specific microscopic etch rates r_i by

$$R = \sum_{i=1}^{N} \rho_i r_i = \sum_{i=1}^{N} \rho_i A_i e^{-E_i/k_B T} \tag{12}$$

Even if the preexponential factors are roughly equal, the macroscopic activation barrier will be still be determined by the relatively complicated equation

$$E_a = -\frac{1}{R}\frac{\partial}{\partial(1/k_B T)} R = \frac{\sum_{i=1}^{N} \rho_i E_i e^{-E_i/k_B T}}{\sum_{i=1}^{N} \rho_i e^{-E_i/k_B T}} \tag{13}$$

Since the site-dependent activation barriers enter this equation exponentially, sites with a low activation barrier (e.g., defects) will have a disproportionate effect on the macroscopic barrier.

To further investigate the correlation between macroscopic and microscopic activation barriers, we have performed atomistic kinetic Monte Carlo simulations of etching, which will be described in detail in an upcoming publication.[59] In most of the cases we simulated, the macroscopic activation barrier obtained from an Arrhenius analysis of a single miscut surface is temperature-dependent and poorly correlated to the microscopic barriers. On the bases of these simulations, we predict that the actual activation barrier to Si(111) terrace site etching is significantly *larger* than 0.65 eV (the largest macroscopic barrier) and that the barrier to etching of the most reactive defect site, which is possibly the kink site, is significantly *smaller* than 0.56 eV, the smallest macroscopic barrier. These predictions are in qualitative agreement with eq 10.

In summary, temperature-dependent measurements of the etch anisotropy show that etching of silicon by KOH cannot be adequately described by a single activation barrier. This reaction displays markedly non-Arrhenius behavior which we attribute to the multisite nature of etching reactions. The orientation of the Si(110) rough-to-smooth transition, which is correlated with an apparent discontinuity in the etch rate, is highly temperature dependent, even near room temperature. This temperature dependence implies a low activation barrier that is inconsistent with a structural transition.

D. KOH Concentration Dependence. In an attempt to further elucidate both the chemical mechanism of KOH/Si etching, as well as the origins of the etch rate discontinuity, we measured the concentration dependence of the etchant anisotropy in a variety of 70 °C KOH solutions. Identically scaled polar plots of these results are displayed in Figure 12a−f. The concentration dependence is both orientation-dependent and rather complicated. Interestingly, the minimum etch rate for most orientations occurs at the highest KOH concentration studied: 50%; however, most orientations also show a local minimum at 12.5% as well. In contrast, most, but not all, surfaces showed a maximum etch rate at 7.9%.

Given the unusual concentration dependence as well as the secondary minimum at 12.5%, questions about experimental error and reproducibility immediately arise. To allay these concerns, Figure 13 shows the raw data for 6 different experiments: replicate runs at 7.9%, 12.5%, and 19.8% KOH. Clearly, the run-to-run reproducibility for this technique is quite good, and experimental error cannot account for the secondary minimum at 12.5% KOH.

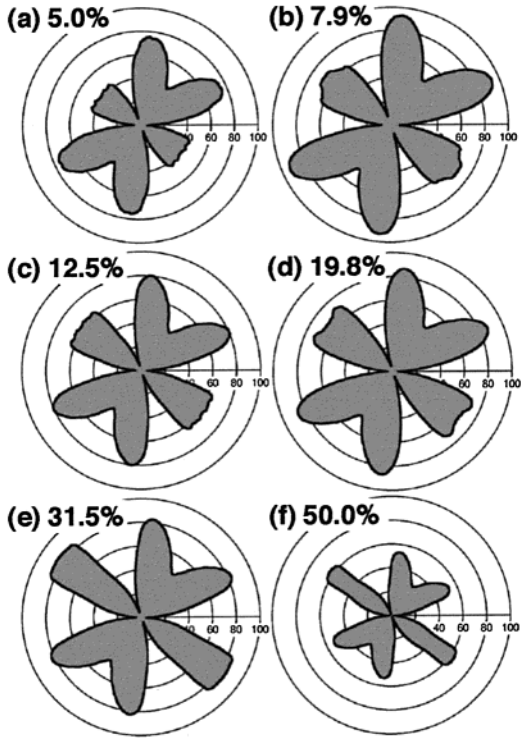

Figure 12. Concentration-dependent etch rates of silicon in a variety of 70 °C KOH solutions. The etch rates are in μm/h, and the horizontal axis denotes the Si(111) face at $\phi = 0°$.

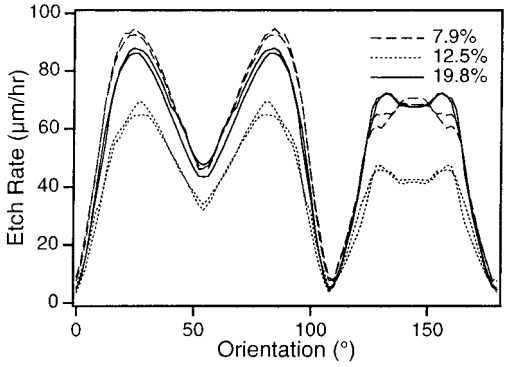

Figure 13. Replicate etch rate measurements in 7.9% KOH, 12.5% KOH, and 19.8% KOH at 70 °C demonstrate the reproducibility of this technique.

The rate of most chemical reactions can be described, at least over modest concentration ranges, by an empirical rate law that scales as the concentration of the reactants raised to a small power (e.g., 1, 2, 0.5).[60] For this reaction, an empirical rate law of the form

$$R(\phi) = k[OH^-]^a[H_2O]^b \tag{14}$$

is expected, where k, a, and b are constants that may be orientation dependent. The constant k is primarily determined by the activation barriers, as discussed in the previous section, whereas the constants a and b contain information about the molecularity of the elementary steps and thus about the reaction mechanism.

In principle, each of the different orientations can be analyzed to obtain estimates of the constants k, a, and b; however, a brute force approach of this type is error-sensitive and difficult to interpret. Most of the variation in the etch rates with orientation is due to the (macroscopic) activation barriers, which are better

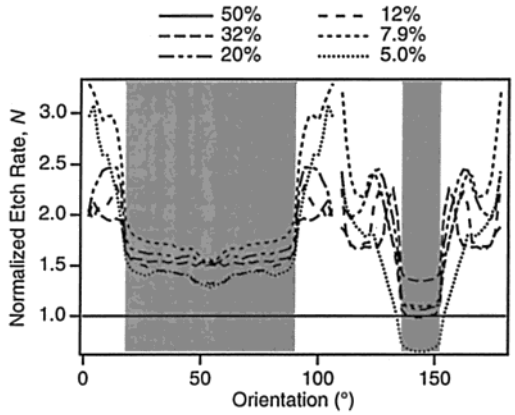

Figure 14. The concentration-dependent rates of silicon etching normalized to the 50% KOH etch rate. The shaded areas represent the regions of smooth etch morphology in 50% KOH. For each concentration, the relative rates of etching are roughly constant across each shaded region; however, the rates of each region are concentration dependent.

studied by varying temperature, not concentration. To isolate the dependence on molecularity, we normalized each orientation-dependent etch rate to the corresponding rate in 50% KOH. The normalized etch rates, $N(\phi)$, are plotted in Figure 14 and should be given by

$$N(\phi) = \left(\frac{[OH^-]}{8.91\ M}\right)^a \left(\frac{[H_2O]}{47.5\ M}\right)^b \qquad (15)$$

if an empirical model is correct. (The concentrations of OH^- and H_2O in 50% KOH are 8.91 and 47.5 M, respectively.[12])

The normalized etch rates in Figure 14 show that all vicinal Si(100) surfaces and all low miscut Si(110) surfaces display the same concentration dependence regardless of miscut. Moreover, the boundaries between these regions of similarity also correspond to the morphological transitions, as shown by the shaded areas. This again suggests that the surfaces are divided into three, or possibly four, regions of similar reactivity: the Si(100) region, the Si(110) region, and one or two regions of Si(111) step flow etching. These are *the same four regions* of reactivity that were suggested by the isotopic substitution experiments described in section B.

The large variations in the vicinal Si(111) data are primarily due to the low etch rates of these surfaces. Since vicinal Si(111) surfaces are well fit by the simple step flow model, we simplified these data by fitting them to eq 3 and extracting the rates of $\langle 11\bar{2}\rangle$ and $\langle \bar{1}\bar{1}2\rangle$ step etching. Figure 15 shows the normalized, concentration-dependent rates of Si(111) step etching as well as the averaged normalized rates of the (100) and (110) regions.

The data in Figure 15 cannot be credibly fit to an empirical rate law of the form given in eq 14. In particular, the secondary minimum at 12.5% KOH is irreproducible. Even when a "best fit" is calculated, the fit parameters are unphysical. For example, *b*, the water exponent, has a value between 5 and 7, which implies penta- to heptamolecular collisions!

Of course, at the high KOH concentrations used in these experiments, rate laws should be cast in terms of activities, not concentrations. The activity of KOH solutions as a function of concentration has been determined electrochemically;[61] however, the effects of this correction are small in solutions below ~30% w/v. When we replaced $[OH^-]$ with experimentally determined values of a_{OH-} in our fits, no improvement was seen.

Glembocki and co-workers[11] previously observed an etch rate maximum at intermediate KOH concentration for Si(100)

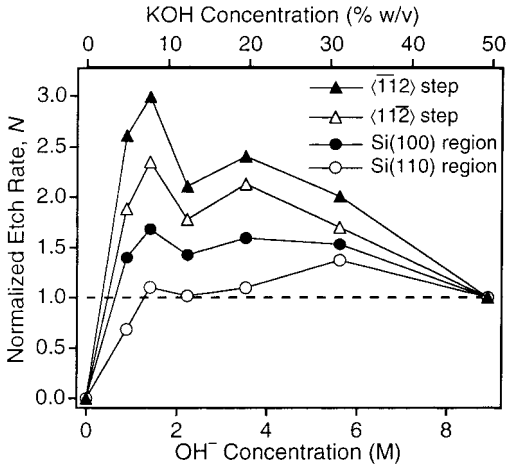

Figure 15. The normalized, concentration-dependent rates of KOH etching fall into four regions of reactivity, as shown by Figure 14. The average behavior of each region is plotted. The reactivity of the $\langle 11\bar{2}\rangle$ and $\langle \bar{1}\bar{1}2\rangle$ steps were obtained from best fits of vicinal Si(111) surfaces ($\phi > 108°$ and $\phi < 108°$, respectively) to eq 3.

surfaces which they attributed to the difference in reactivity between free and bound water molecules. Since water molecules in the first hydration shell of OH^- are presumably less reactive than free H_2O molecules, they suggested an empirical rate law of the form

$$R(\phi) = k[OH^-]^a([H_2O] - m[OH^-])^b \qquad (16)$$

where *m* is the average number of H_2O molecules bound to each OH^- ion. This modification does not improve the fit to our data, however. If the fit is forced, we find a best fit of $m = 5.1 \pm 0.9$ with (a, b) in the range of $(0-0.1, 0.2-0.3)$, depending on orientation. Although the hydration number is reasonable,[11] the exponents in the empirical rate law appear to be unphysical.

In our opinion, the complicated concentration dependence of the four regions of KOH etching *cannot be explained or fit* by a simple empirical rate law. This breakdown is most likely attributable to the multisite nature of macroscopic surface etching. SEM micrographs clearly show that the etch morphology is concentration dependent. As a result, the individual site densities must also be concentration dependent. Even if all of the site-specific chemical reactions obey empirical rate laws of the form given in eq 14, the macroscopic etch rate need not follow a similar law.

The complicated concentration dependence of vicinal Si(111) etching, which is represented by the triangles in Figure 15, is somewhat surprising. The derivation of eq 3 was based on arguments about the existence of a single, fast etching step etch site (e.g., a step or kink site). Although this simple model reproduces the etch rates well, it cannot explain either the bunched surface morphologies discussed in Section A or the complicated concentration dependence in Figure 15. These discrepancies underscore the necessity of microscopic studies (e.g., STM or AFM) of the evolution of the etch morphology.

IV. Conclusions

Although the KOH etching of silicon leads to complicated dependencies on many variables, the magnitude of the kinetic isotope effect, the morphology of the macrosteps on vicinal Si(111) surfaces, the pronounced hydrophobicity of the etched surfaces and the H-termination of the etched surfaces are all consistent with a chemical mechanism that is rate-limited by

the cleavage of a Si−H bond by OH^- (reaction 9). The orientation-resolved kinetic data cannot be explained by a single-site model of chemical etching; the multisite nature of the etching surface complicated the macroscopic etch rate. There is, however, no evidence of a gross change of chemical mechanism with surface orientation.

The etch rates of silicon surfaces are highly dependent on surface orientation, reaction temperature, and KOH concentration. In general, these etch rates are *poorly fit* to standard models of chemical reactivity. The temperature dependence is markedly non-Arrhenius in nature, and the etch anisotropy actually *increases* with temperature. The KOH concentration dependence cannot be fit by simple empirical rate laws. These effects are attributed to the multisite nature of the etching reactions. Etching reactions often occur preferentially at surface defects. Also, the act of chemical etching changes both the surface morphology and the distribution of reactive sites on the surface. Because of this, the kinetics of a macroscopic surface are not dominated by the reactivity of the majority species: the terrace site. Even if all reactive species on the etching surface rigorously obey the expected kinetic laws (e.g., the Arrhenius equation), the macroscopic etch rate will be determined by a complicated temperature and concentration-dependent average over the reactive species. This averaging process leads to a breakdown of the standard kinetic laws at the macroscopic level.

In contrast, studies of the *macroscopic* kinetic isotope effect are much less affected by morphological changes in the surface (whether due to miscut or etching), because these measurements involve the ratioed etch rates of surfaces that have similar or identical morphologies.

The reactivity of silicon surfaces can qualitatively be divided into four regions of similarity: vicinal Si(100) surfaces, vicinal Si(110) surfaces, vicinal Si(111) surfaces miscut toward the $\langle 11\bar{2} \rangle$ direction, and vicinal Si(111) surfaces miscut toward the $\langle \bar{1}12 \rangle$ direction. Within each region, the surfaces display remarkably similar chemical kinetics. Each region has a characteristic temperature, concentration and isotope dependence as well as a characteristic etch morphology. The transition between the regions leads to apparent discontinuities in both the etch rates and in the etch morphologies. The orientation of the transition between the regions is well-defined, but temperature dependent.

The etch rates of vicinal Si(111) surfaces are well fit by a simple step flow etching model at all of the KOH concentrations and reaction temperatures studied. This fit implies that step etching dominates the reactivity of these surfaces and that the individual steps etch with a step-density-independent rate. According to current theories of macrostep formation, these kinetics should prevent macrostep formation. Nevertheless, large macrosteps form on these surfaces.

Low-miscut Si(110) surfaces etch with an orientation-independent (i.e. isotropic) etch rate. Although this isotropy would seem to imply atomic scale isotropy, this is not the case. The orientation-independent etch rate can be explained by etching-induced faceting, which has been observed using SEM imaging. The chemical origins of this faceting are not understood, and further atomic scale studies of this are also needed.

In summary, orientation-resolved studies of surface etching have been shown to provide much more information and chemical insight than kinetic studies of single surfaces. Despite its seeming simplicity, though, KOH etching of silicon is a surprisingly complex reaction.

Acknowledgment. We thank Yi-Chiau Huang for supplying the STM micrographs in Figure 5. M.A.H. is a Cottrell Scholar of the Research Corporation, and R.A.W. thanks the Corning Foundation for fellowship support. This material was supported in part by the NSF under Award CHE-9733165 and by the MRSEC Program of the NSF under Award DMR-9632275. This work was performed in part at the Cornell Nanofabrication Facility (a member of the National Nanofabrication Users Network) which is sponsored by the NSF under Award ECS-9319009, Cornell University, and industrial affiliates.

References and Notes

(1) Bassous, E.; Baran, E. F. *J. Electrochem. Soc.* **1978**, *125*, 1321.
(2) Chang, P.-Z.; Yang, L.-J. *J. Micromech. Microeng.* **1998**, *8*, 182.
(3) Seidel, H.; Csepregi, L.; Heuberger, A.; Baumgärtel, H. *J. Electrochem. Soc.* **1990**, *137*, 3612.
(4) Wind, R. A.; Hines, M. A. *Surf. Sci.* **2000**, *460*, 21.
(5) Rappich, J.; Lewerenz, H. J.; Gerischer, H. *J. Electrochem. Soc.* **1993**, *140*, L187.
(6) Pietsch, G. J.; Chabal, Y. J.; Higashi, G. S. *Surf. Sci.* **1995**, *331*, 395.
(7) Pietsch, G. J.; Chabal, Y. J.; Higashi, G. S. *J. Appl. Phys.* **1995**, *78*, 1650.
(8) Weldon, M. K.; Queeney, K. T.; Gurevich, A. B.; Stefanov, B. B.; Chabal, Y. J.; Rahghavachari, K. *J. Chem. Phys.* **2000**, *113*, 2440.
(9) Alay, J.-L.; Verhaverbeke, S.; Vandervorst, W.; Heyns, M. *J. Appl. Phys.* **1993**, *32*, 358.
(10) Palik, E. D.; Bermudez, V. M.; Glembocki, O. J. *J. Electrochem. Soc.* **1985**, *132*, 871.
(11) Glembocki, O. J.; Palik, E. D.; de Guel, G. R.; Kendall, D. L. *J. Electrochem. Soc.* **1991**, *138*, 1055.
(12) In this manuscript, all concentrations reported as a percentage are w/v, not w/w, unless noted otherwise. Conversions between KOH molarity, molality, w/w and w/v were performed with data from *The CRC Handbook of Chemistry and Physics*, 56th ed.; Weast, R. C., Ed.; CRC Press: Cleveland, 1975; p D-244.
(13) Frank, F. C. In *Growth and Perfection of Crystals*; Doremus, R. H., Roberts, B. W., Turnbull, D., Eds.; Wiley: New York; 1958; p 4113.
(14) Cabrera, N.; Vermilyea, D. A. In *Growth and Perfection of Crystals*; Doremus, R. H., Roberts, B. W., Turnbull, D., Eds.; Wiley: New York; 1958; p 393.
(15) Lighthill, M. J.; Whitham, G. B. *Proc. R. Soc. London A* **1955**, *229*, 281.
(16) Heimann, R. B. In *Crystals: Growth, Properties, and Applications*; Grabmaier, J., Ed.; Springer-Verlag: Berlin; 1982; Chapter 4.
(17) Huang, Y.-C.; Flidr, J.; Newton, T. A.; Hines, M. A. *J. Chem. Phys.* **1998**, *109*, 5025.
(18) Duport, C.; Noziéres, P.; Villain, J. *Phys. Rev. Lett.* **1995**, *74*, 134.
(19) Kukta, R. V.; Battacharya, K. *Thin Solid Films* **1999**, *357*, 35.
(20) Shenoy, V. B.; Zhang, S.; Saam, W. F. *Surf. Sci.* **2000**, *467*, 58.
(21) Larsson, M. I. *Phys. Rev. B* **1997**, *56*, 15157.
(22) Bales, G. S.; Zangwill, A. *Phys. Rev. B* **1990**, *41*, 5500.
(23) Vladimirova, M.; Pimpinelli, A.; Videcoq, A. *J. Cryst. Growth* **2000**, *220*, 631.
(24) Videcoq, A.; Pimpinelli, A.; Vladimorova, M. *Appl. Surf. Sci.* **2001**, *177*, 213.
(25) Latyshev, A. V.; Aseev, A. L.; Krasilnikov, A. B.; Stenin, S. I. *Surf. Sci.* **1989**, *213*, 157.
(26) Kandel, D.; Weeks, J. D. *Phys. Rev. Lett.* **1995**, *74*, 3632.
(27) Williams, E. D.; Fu, E.; Yang, Y.-N.; Kandel, D.; Weeks, J. D. *Surf. Sci.* **1995**, *336*, L46.
(28) Fu, E. S.; Liu, D.-J.; Johnson, M. D.; Weeks, J. D.; Williams, E. D. *Surf. Sci.* **1997**, *385*, 259.
(29) Liu, D.-J.; Weeks, J. D.; Kandel, D. *Phys. Rev. Lett.* **1998**, *81*, 2743.
(30) v. d. Eerden, J. P.; Müller-Krumbhaar, H. *Phys. Rev. Lett.* **1986**, *57*, 2431.
(31) v. d. Eerden, J. P.; Müller-Krumbhaar, H. *Phys. Scr.* **1989**, *40*, 337.
(32) Kandel, D.; Weeks, J. D. *Phys. Rev. Lett.* **1992**, *69*, 3758.
(33) Kandel, D.; Weeks, J. D. *Phys. Rev. B* **1994**, *49*, 5554.
(34) Nijdam, A. J.; van Veenendaal, E.; Cuppen, H. M.; van Suchtelen, J.; Reed, M. L.; Gardeniers, J. G. E.; van Enckevort, W. J. P.; Vlieg, E.; Elwenspoek, M. *J. Appl. Phys.* **2001**, *89*, 4114.
(35) Phaneuf, R. J.; Bartelt, N. C.; Williams, E. D.; Swiech, W.; Bauer, E. *Phys. Rev. Lett.* **1991**, *67*, 2986.
(36) Hibino, H.; Ogino, T. *Phys. Rev. Lett.* **1994**, *72*, 657.
(37) Jeong, H.-C.; Weeks, J. D. *Phys. Rev. B* **1998**, *57*, 3939.
(38) Khare, S. V.; Einstein, T. L.; Bartelt, N. C. *Surf. Sci.* **1995**, *339*, 353.
(39) Hines, M. A. *Int. Rev. Phys. Chem.* **2001**, *20*, 645.
(40) Flidr, J.; Huang, Y.-C.; Hines, M. A. *J. Chem. Phys.* **1999**, *111*, 6970.

(41) Smith, R. L.; Collins, S. D. *J. Appl. Phys.* **1992**, *71*, R1.
(42) Baum, T.; Schiffren, D. J. *J. Electroanal. Chem.* **1997**, *236*, 239.
(43) Carpenter, B. K. *Determination of Organic Reaction Mechanisms*; Wiley: New York, 1984; Chapter 5.
(44) Luo, H.; Chidsey, C. E. D. *Appl. Phys. Lett.* **1998**, *72*, 477.
(45) Mills, R.; Lobo, V. M. M. *Self-diffusion in Electrolyte Solutions*; Elsevier: Amsterdam, 1989; p 318.
(46) Armitage, D. A. In *Comprehensive Organometallic Chemistry*; Wilkinson, G., Ed.; Pergamon: Oxford, 1982; Vol. 2, p 1.
(47) Rochow, E. G. In *Comprehensive Inorganic Chemistry*; Bailar, J. C., Jr., Emeléus, H. J., Nyholm, R., Eds.; Pergamon: Oxford, 1973; Vol. 1, p 123.
(48) Holmes, R. R. *Chem. Rev.* **1990**, *90*, 17.
(49) Hajdasz, D. J.; Squires, R. R. *J. Am. Chem. Soc.* **1986**, *108*, 3139.
(50) Jakob, P.; Chabal, Y. J. *J. Chem. Phys.* **1991**, *95*, 2897.
(51) Pehlke, E.; Tersoff, J. *Phys. Rev. Lett.* **1991**, *67*, 1290 and references therein.
(52) Williams, E. D.; Phaneuf, R. J.; Wei, J.; Bartelt, N. C.; Einstein, T. L. *Surf. Sci.* **1993**, *294*, 219.
(53) Sander, M.; Imbihl, R.; Ertl, G. *J. Chem. Phys.* **1992**, *97*, 5193.
(54) Mönch, W. *Semiconductor Surfaces and Interfaces*; Springer-Verlag: Berlin, 1993; Chapter 12.
(55) Zimmermann, F. M.; Pan, X. *Phys. Rev. Lett.* **2000**, *85*, 618.
(56) Reider, G. A.; Höfer, U.; Heinz, T. F. *J. Chem. Phys.* **1991**, *94*, 4080.
(57) Herr, E.; Baltes, H. *Sens. Actuators, A* **1992**, *31*, 283.
(58) Yun, M. H.; Burrows, V. A.; Kozicki, M. N. *J. Vac. Sci. Technol B* **1998**, *16*, 2844.
(59) Wind, R. A.; Hines, M. A. In preparation.
(60) Noggle, J. H. *Physical Chemistry*; Harper-Collins; New York, 1996; Chapter 10.
(61) Akerlof, G. C.; Bender, P. *J. Am. Chem. Soc.* **1948**, *70*, 2366.